

Conditional Generative Modelling of Reconstructed Particles at Collider Experiments

Francesco Armando Di Bello¹, Etienne Dreyer², Sanmay Ganguly³,
Eilam Gross², Lukas Heinrich⁴, Marumi Kado^{4,5}, Nilotpal Kakati²,
Jonathan Shlomi², Nathalie Soybelman²

¹ University of Genova

² Weizmann Institute of Science

³ ICEPP, University of Tokyo

⁴ Technical University of Munich

⁵ Sapienza University of Rome

E-mail: nathalie.soybelman@weizmann.ac.il, nilotpal.kakati@weizmann.ac.il

November 2022

Abstract. The simulation of particle physics data is a fundamental but computationally intensive ingredient for physics analysis at the Large Hadron Collider, where observational set-valued data is generated conditional on a set of incoming particles. To accelerate this task, we present a novel generative model based on a graph neural network and slot-attention components, which exceeds the performance of pre-existing baselines.

Keywords: fast simulation, transformer, graph networks, slot-attention, conditional generation

1. Introduction

One of the most computationally expensive tasks in high-energy physics at collider experiments is the simulation and reconstruction of collision events. Simulation tools such as Geant4 [1] use microphysical models to simulate the detailed stochastic interactions of a variable-sized *set* of “truth” particles $T = \{t_i | i = 1 \dots N_T\}$ with the detector material producing a set of signals (“hits”) H in the read-out sensors of the detector. This simulation implicitly corresponds to an underlying distribution $p_{\text{sim}}(H|T)$. As modern detectors have up to a hundred million of such sensors, the high-dimensional space of hits is inconvenient for physics analysis. “Reconstruction” is a deterministic inference algorithm $R(H)$ that attempts to recover approximately the set-valued latent input T to present physicists with an interpretable and low-dimensional summary of the hit data as a set of *reconstructed* particles $R = \{r_i | i = 1 \dots N_R\}$ that aims to approximate T . Typically, physicists do not directly interact

with the hit-level data, but only with the effective set-valued model

$$R \sim p(R|T) = \int dH \delta(R(H) - R) p_{\text{sim}}(H|T). \quad (1)$$

Due to the high computational cost of both simulation and reconstruction there is considerable interest in exploiting generative machine learning to develop fast surrogates for this effective model. In this work, we explore the possibility to train an end-to-end surrogate $R \sim q_{\theta}(R|T)$ with learnable parameters θ . We split the generative process into a cardinality prediction task $q_{\theta_1}(N_R|T)$ and a doubly conditional set generation task $q_{\theta_2}(R|N_R, T)$. The necessary permutation invariances implied by the set nature of T and R are enforced through inductive biases in the architecture. Our results exceed the performance of baseline models.

1.1. Related Work

There are two main approaches to approximate $p(R|T)$. In one approach only $p_{\text{sim}}(H|T)$ is replaced by a fast surrogate such as CaloGAN [2]. Based on its output, the standard reconstruction algorithm may be used to produce reconstructed particle sets $R(H)$. This approach has two disadvantages: Firstly, the surrogate must correctly learn a high-dimensional generative model $H \sim p(H|T)$ only for H to be further processed and reduced in dimension to form reconstructed events. Secondly, this approach incurs the full cost of the standard reconstruction, which is still significant. The second approach aims for a direct approximation of the lower-dimensional $p(R|T)$. Prior work simplifies the problem by first projecting the sets to fixed-sized feature vectors of the truth and reconstructed events $\mathbf{t} = f_t(T)$, $\mathbf{r} = f_r(R)$, and aims to learn a fast generative model $p(\mathbf{r}|\mathbf{t})$ [3–5]. This approach is limited by the *fixed* choice of f_r, f_t and thus does not enable one to generate features outside of f_r . A fully general approach modelling $p(R|T)$ is only possible through a *set-to-set* approach. Prior work has aimed at learning a fast surrogate using a set-valued variational autoencoder (VAE) [6], similar to the baseline we present in this work. The encoder yields a latent distribution $p(z|T)$, and a decoder implements a model of reconstructed events $p(R|z)$. While this model successfully reproduces the *marginal* distributions (i.e. projections of $p(R) = \int dT p(R|T)p(T)$), the authors note that “[the algorithm] fails in faithfully describing the jet dynamics at constituents level” and do not present non-marginal results. To the best of our knowledge, this is the first work presenting an extensive analysis of the conditional distribution of such a set-to-set model in a particle physics application.

2. Dataset

We demonstrate the set-to-set approach using a simplified ground truth model of $p(R|T)$ for charged elementary particles represented by their direction and momentum features $(p_{\text{trans.}}, \eta, \phi)$. In order to learn the cardinality and conditional set generation models $q(N|T)$ and $q(R|T, N)$ we generate a set of representative truth events. For each truth event, we generate multiple samples of the target distribution $\mathcal{D} = \{R_j, T_j\} \sim p(R_i|T_j)p(T_j)$ resulting from simulation and subsequent reconstruction. In particular, we generate several

reconstructions R , referred to as *replicas* for the same truth event T . The replica cardinalities N then serve as labels for the supervised training of the cardinality prediction, while the conditional empirical distribution of replicas for a given truth event serves as training samples for the unsupervised set generation task.

2.1. Truth Event Generation

In the present work, we focus on a localized reconstruction of particles within a single jet. Events are produced using Pythia8 [7] to generate a single quark with momentum between 10 GeV and 200 GeV with subsequent parton shower and hadronization. The quark’s initial direction is randomly chosen in the ranges $|\eta| < 2.5$ and $|\phi| < \pi$. Stable particles with momentum above 1 GeV and $|\eta| < 3.0$ are clustered based on their four-momenta through the anti- k_T algorithm [8] and the leading jet is selected. After clustering, we isolate the charged particles removing the neutrals. The set of charged particles inside the jets has an average cardinality of $N_{\text{ch}} = 3.72$ with a maximum of 12 particles and a minimum of 1 particle per truth event. The training, validation, and test data set consist of 2915, 500, and 3990 truth events respectively. For training (evaluation) 25 (100) independent reconstructions are generated per truth event.

2.2. Tracking emulation and smearing

Each of the charged particles in the generated truth event is assumed to be generated at the origin. The trajectory of the charged particle through the inner detector, i.e. track, is parameterized by five perigee parameters which are called a_0 , z_0 , q/p , θ , ϕ . Here q and p are the charge and magnitude of the three-momentum of the associated particle. θ and ϕ parameterise the unit vector along the momentum direction. a_0 and z_0 are associated with the track curvature. The effect of reconstruction of charged particles is emulated by smearing the q/p , θ , and ϕ values of their associated track. Each is independently varied by a Gaussian resolution model with width dependent on the transverse momentum of the charged particle. Additionally, a deterministic model is used to introduce tracking inefficiency. Charged particles are dropped if they were produced far from the beamline in terms of transverse radius R ($R > 75$ mm for $|\eta| < 1.5$ and $R > 250$ mm otherwise). This results in an efficiency of $95.3 \pm 0.8\%$ over the combined training, validation, and test dataset.

3. Models and Training

In this work, we compare a novel neural network architecture based on a graph neural network and slot-attention to a baseline model in the form of a conditional variational auto-encoder. In the following, we briefly describe the model architectures and training process for both models.

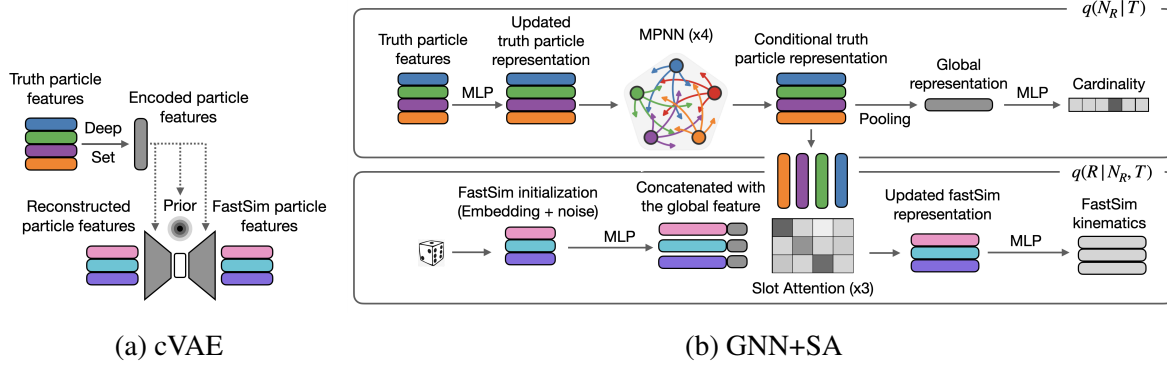


Figure 1: Architectures of the two models

3.1. Conditional VAE

For the baseline results, we train a conditional variational auto-encoder [9] to approximate the distribution $p(R|T)$ by a variational model q_ϕ . For this we extend the typical construction of variational auto-encoders [10] by conditioning the prior $q_P(z|T)$, an encoder $q_E(z|R, T)$ and a decoder $q_D(R|z, T)$ on the truth event T . As both R and T are sets, we encode them as Deep Sets [11] before passing them into the encoder and prior to ensure permutation invariance. To handle the variable number of input particles, the cVAE input is zero-padded to a maximum cardinality and the output of the decoder network includes an additional presence variable, to indicate whether the corresponding vector is to be considered a member of the output set. The threshold value for the presence variable was optimized through a grid search to 0.6. A sketch of the cVAE architecture is shown in Figure 1a. To generate reconstructed events R , a latent code is sampled from the conditional prior $z \sim q_P(z|T)$ which is then passed through the decoder to produce candidate output vectors. The presence of each particle is then sampled according to its indicator variable.

3.2. Graph Neural Network and Slot-Attention Model

In addition to the cVAE, we present results on a novel model that uses a combination of graph neural networks and slot-attention layers [12]. The general strategy is to use a graph neural network with message passing to encode the truth particles T into a high-dimensional vector representation $\{t'_i\}$, predict the corresponding cardinality N_R of the reconstructed event, and finally generate the reconstructed event R at the predicted cardinality by transforming noise vectors into hidden representations of the reconstructed particles from which per-particle attributes such as p_{trans} can be projected out using simple MLP networks as shown in Figure 1b. The first step corresponds to a model $q_{\theta_1}(N_R|T)$, whereas the second implements the model $q_{\theta_2}(R|N_R, T)$.

3.2.1. Input Set Encoding and Cardinality Prediction This embedding is constructed through a fully connected Graph Neural Network, with one node per truth particle. The truth particle attributes $\{p_{trans.}, \eta, \phi\}$ are embedded using a multilayer-perceptron (MLP) and

attached as node features. Once initialized, the graph undergoes multiple rounds of message passing to produce a final set of input feature vectors $\{f_i\}$. A graph-level permutation-invariant pooling operation provides an overall embedding $F(T)$ of the input truth event T . Given the graph-level embedding of the truth event T , the categorical distribution of the output set cardinality is predicted using a simple MLP head. The embedding and cardinality prediction architecture is shown in the top half of Figure 1b.

3.2.2. Conditional Set Generation The model for the output set generation for a fixed cardinality $q_{\theta_2}(R|N_R, T)$ is designed as a generative model transforming a set of noise vectors $\{\varepsilon_i\}$, $i = 1 \dots N_R$ into a set of reconstructed particle featured vectors $R = \{r_i\} = f_\phi(\{\varepsilon_i\})$. The architecture thus encodes an *implicit* model $q(R|N_R, T)$, from which reconstructed events can be sampled even if an explicit evaluation of the likelihood is not possible. In addition to the noise input, the conditional model is provided the final truth particle embedding and the global graph-level encoding of the event $F(T)$ through a set of concatenated input vectors $\{\text{cat}(f_i, F(T))\}$. The output generation proceeds through a Slot Attention layer, in which the vectors corresponding to the output particles are represented as randomly initialized slots that attend over the provided truth particles through multiple rounds of iterative refinement. As an attention mechanism standard query, key and value embedding are used to update the reconstructed particle representation. Here key and value are MLPs that take the truth particle representation as input, while query takes the noise with the global representation. The elements of the attention matrix are calculated by taking the dot-product of key and query. To update the reconstructed set representation, the value is multiplied with the attention matrix, send through a GRU cell and an additional MLP, and added to the initial feature vector. In total 3 rounds of slot attention updates are applied. The output finally provides high-dimensional embeddings of the reconstructed particles from which attributes are projected out using an element-wise MLP. The set generation architecture is sketched in the lower half of Figure 1b. The slot-attention mechanism is permutation-equivariant and thus if the initial noise model is permutation invariant the implicit model learned during training will be as well.

3.3. Training

Generalizing from the non-conditional VAE case, we train the cVAE on the negative evidence lower bound loss (*ELBO*) as averaged over both observed reconstructions R and conditioning values T :

$$\begin{aligned} L &= -\mathbb{E}_{T,R} \mathbb{E}_{z \sim q_E(z|R,T)} \log \frac{q_D(R|z,T) q_P(z|T)}{q_E(z|R,T)} \\ &= -\mathbb{E}_{T,R} \mathbb{E}_z \log q_D(R|z,T) + D_{\text{KL}}(q_E(z|R,T) || q_P(z|T)) \end{aligned} \quad (2)$$

As shown above, the ELBO loss for a given (R, T) pair can be decomposed into two components: the reconstruction loss $\mathbb{E}_{z \sim q_E(z|R,T)} \log q_D(R|z,T)$ and a regularizing term comparing the (now truth-dependent) prior $q_P(z|T)$ to the per-instance posterior $q_E(z|R,T)$ distribution through the Kullback-Leibler divergence. The reconstruction loss is taken to be

the sum of distances in feature space $(p_{trans.}, \eta, \phi)$ after a particle-by-particle assignment through the Hungarian Algorithm [13]. The KL divergence can be computed in closed form as both the posterior $q_E(z|R, T)$ and the prior $q_P(z|T)$ are taken to be multivariate normal distributions with a diagonal covariance matrix Σ . Their respective distribution parameters μ and $\log \Sigma$ are computed through MLPs as a function of their respective conditioning values. We train for 500 epochs (7 hours). The GNN+SA model is trained on a combination of two tasks: cardinality prediction and set generation. The cardinality prediction is trained on a standard categorical cross-entropy loss $L_{card.}$ in expectation over all truth events T . As the model does not provide a tractable likelihood $q_\phi(R|T, N)$, we formulate a sample-based similarity measure between the two distributions $q_\phi(R|T, N)$ and $p(R|T, N)$. A suitable metric is the maximum mean discrepancy (MMD²) [14] which is based on kernel functions $k(x, x')$, which act as a similarity measure between instances. We use the Hungarian Cost as the similarity measure.

$$\text{MMD}^2 = \mathbb{E}_{(x \sim p, x' \sim p)}[k(x, x')] + \mathbb{E}_{(x \sim q, x' \sim q)}[k(x, x')] - 2\mathbb{E}_{(x \sim q, x' \sim p)}[k(x, x')] \quad (3)$$

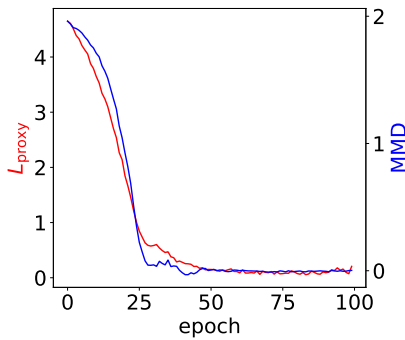


Figure 2: Evolution of MMD and L_{proxy} during training

While the MMD metric enjoys strong theoretical guarantees, such as vanishing when $p = q$, we observed empirically, that training directly on it as a loss converges poorly. We thus use a heuristic proxy loss which facilitates training and empirically correlates well with the MMD, which we track during training as a metric. In Fig. 2 we show that minimizing the proxy loss also minimizes the tracked MMD. In this proxy, we use the minimum kernel entry $L_{\text{proxy}} = \min_{x_i, x'_j} k(x_i, x'_j)$, where x_i is a member of the reference set and x'_j is from the generative model sampling. It is an upper bound on the final $-2\mathbb{E}_{p, q}[k(x, x')]$ term in the MMD definition. Effectively we perform a second Hungarian Algorithm matching the reconstructed replicas with the target once, additionally to the particle-by-particle assignment.

The total loss $L = L_{\text{card.}} + L_{\text{proxy}}$ is averaged over all truth events T . Due to its expensive computation, we only train for 200 epochs (6 days). Both models are jointly optimized using the Adam optimizer [15].

4. Results

We present results for the conditional generation of reconstructed events of charged particles both in terms of per-particle features as well as collective per-event set-level features. As the ground truth model has a deterministic relationship between the truth event T and output cardinality N_R , we can assess the correctness of the model $p(N|T)$ through a comparison of the accuracy

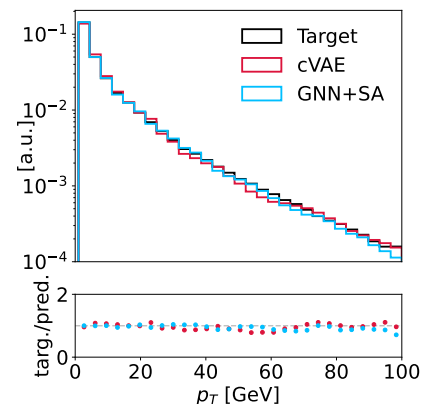


Figure 3: Marginal distribution of per particle observable $p_{trans.}$

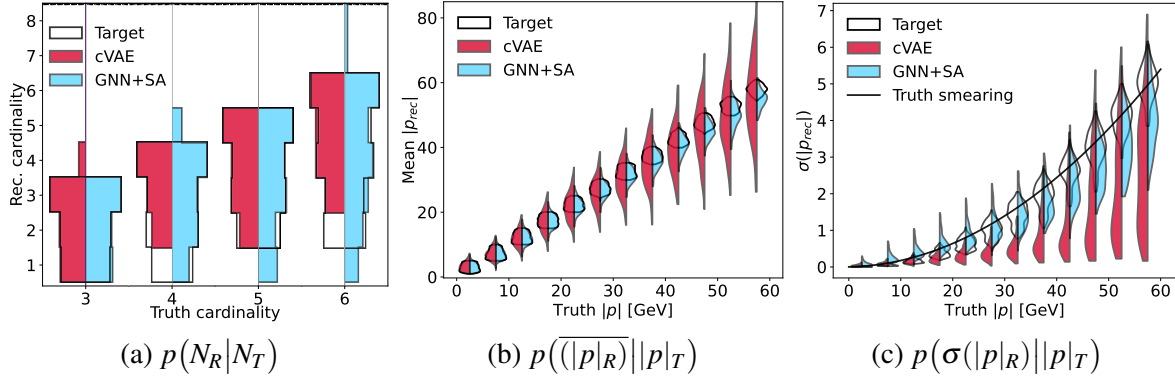


Figure 4: (a) Conditional Cardinality Distribution and (b and c) Distribution of reconstructed particle momentum means and their variances

of the cardinality prediction with the ground-truth cardinality. As shown in Table 1 both models perform similarly after tuning cVAE hyper-parameters. We also observe that marginal distributions are comparably reproduced by both models confirming prior work in this area. Figure 3 shows the per-particle momentum as an example. Differences in the two models begin to emerge when studying projections of the *conditional* distributions $p(R|T)$. We present projected distributions $p(\mathbf{r}|\mathbf{t}) = p(f_r(R) = \mathbf{r}|f_t(T) = \mathbf{t})$, where $f_t(\cdot), f_r(\cdot)$ extract feature vectors on T and R respectively. In Figure 4a, we compare the learned cardinality distributions as a function of the truth cardinality $p(N_R|N_T)$. Both models broadly reproduce the target, however, the GNN+SA achieves better modelling at lower cardinalities. In Figure 4b we compare the per-particle mean reconstructed momentum in bins of truth-momentum. In the ground truth reconstruction, the distribution of reconstructed momenta is as expected centered around the true momenta, with the width reflecting the variance of the noise model and a residual variance contributed to the finite size bin-width in the conditional feature \mathbf{t} . Here we can see that while the GNN+SA model does not fully match the ground truth it performs markedly better than the cVAE model. The high variance of the cVAE model indicates that it does not model the mean of the reconstructed particle distributions correctly. In Figure 4c the same analysis is performed for the variance of the reconstructed feature distribution and compared to the underlying ground-truth noise model that was applied to the truth particles. Here, the difference between the two models becomes even more apparent:

	Accuracy $q(N_R T)$ [%]	MMD ² $q(R N, T)$	Hungarian Cost $C(R, T) \bar{C}_q - \bar{C}_p $
GNN+SA	81.2 ± 0.2	-0.004 ± 0.029	0.026
cVAE	80.5 ± 0.2	0.037 ± 0.037	0.089

Table 1: Performance metrics comparing cardinality prediction accuracy, the MMD metric, and the difference in the mean Hungarian Cost between reconstructed and truth events of the surrogate models to the ground truth.

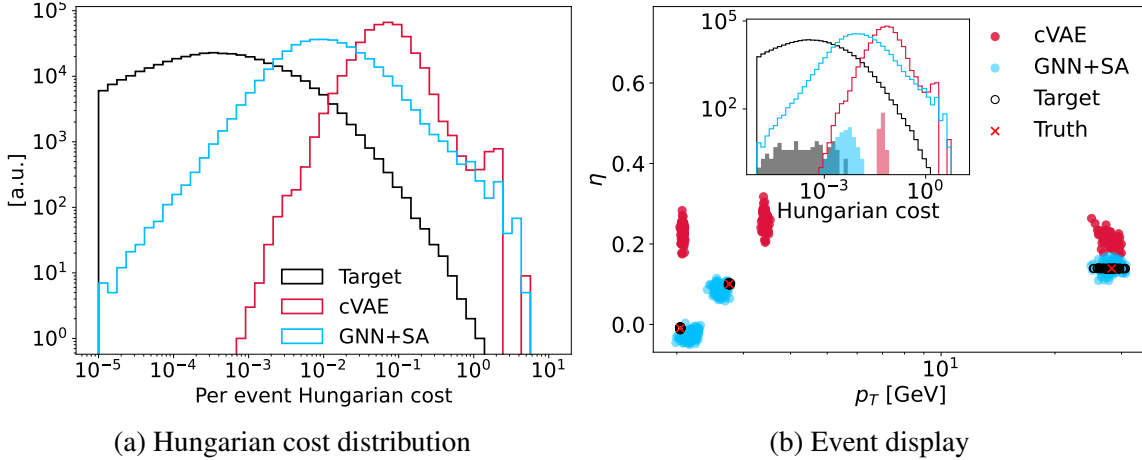


Figure 5: Hungarian cost distribution of the reconstructed events to the truth events and representative event display showing the improved performance of GNN+SA.

Whereas the GNN+SA model does track the ground truth model, albeit, with a degree of under-estimation and increased variance at high momenta, the cVAE model does not manage to correctly capture the momentum dependence of the resolution to a satisfying degree. The failures of the cVAE model are apparent in the representative truth event shown in Figure 5b. Comparing the results in Figure 3 and Figures 4 underlines the importance of a detailed study of the learned set-valued distribution – which is first done in this work – as mismodelling may not be apparent from marginal distributions alone. Finally, we present a metric that aims to distill the interplay between multi-particle correlation as well as the shifts in mean and variance modelling observed in the previous section into a single number. In Figure 5a we show the distribution of the Hungarian Loss $C(R, T)$ of the reconstructed events to the truth events as averaged over the full test set. The mean GNN+SA cost lies much closer to the mean ground-truth cost as compared to the cVAE model. To give a sense of scale for the significant improvement a single event is shown in the main panel of Figure 5b. The cVAE fails to sample reconstructed particles correctly yielding a high Hungarian Cost. The GNN+SA samples resemble the target to a markedly higher degree. The cost distributions for this single truth event are shown as filled histograms in the inset. They each lie in the bulk of the truth-averaged distribution. The shown event is thus a representative example of the model performance. Similarly, the GNN+SA exceeds the cVAE performance as measured by MMD^2 metric as listed in Table 1.

5. Conclusions

We have presented an approach for a set-conditional set generation model to approximate simulation and subsequent reconstruction. We split the task into a two-step generative procedure of cardinality prediction followed by conditional set generation and choose appropriate permutation-invariant architectures through message-passing graph neural networks and slot-attention (GNN+SA). Results are shown on the reconstructions of the

local collection of noised truth particles and compared to a baseline model that uses a cVAE architecture. The GNN+SA model outperforms the baseline model and better captures key properties of the target distribution. Although the results are not yet suitable for a real physics application, they are a significant improvement over the prior state-of-the-art.

Acknowledgement

ED is supported by the Zuckerman STEM Leadership Program. SG is partially supported by Institute of AI and Beyond for the University of Tokyo. EG is supported by the Israel Science Foundation (ISF), Grant No. 2871/19 Centers of Excellence. LH is supported by the Excellence Cluster ORIGINS, which is funded by the Deutsche Forschungsgemeinschaft (DFG, German Research Foundation) under Germany's Excellence Strategy - EXC-2094-390783311.

References

- [1] S. Agostinelli et al. GEANT4: A simulation toolkit. *Nucl. Instrum. Meth.*, A506:250–303, 2003.
- [2] Michela Paganini, Luke de Oliveira, and Benjamin Nachman. CaloGAN : Simulating 3D high energy particle showers in multilayer electromagnetic calorimeters with generative adversarial networks. *Phys. Rev. D*, 97(1):014021, 2018.
- [3] Georges Aad et al. AtlFast3: the next generation of fast simulation in ATLAS. *Comput. Softw. Big Sci.*, 6:7, 2022.
- [4] Anja Butter, Tilman Plehn, and Ramon Winterhalder. How to GAN LHC Events. *SciPost Phys.*, 7(6):075, 2019.
- [5] Raghav Kansal, Javier Duarte, Breno Orzari, Thiago Tomei, Maurizio Pierini, Mary Touranakou, Jean-Roch Vlimant, and Dimitrios Gunopulos. Graph generative adversarial networks for sparse data generation in high energy physics, 2020.
- [6] Mary Touranakou, Nadezda Chernyavskaya, Javier Duarte, Dimitrios Gunopulos, Raghav Kansal, Breno Orzari, Maurizio Pierini, Thiago Tomei, and Jean-Roch Vlimant. Particle-based fast jet simulation at the LHC with variational autoencoders. *Mach. Learn. Sci. Tech.*, 3(3):035003, 2022.
- [7] Torbjorn Sjostrand, Stephen Mrenna, and Peter Z. Skands. A Brief Introduction to PYTHIA 8.1. *Comput. Phys. Commun.*, 178:852–867, 2008.
- [8] Matteo Cacciari, Gavin P. Salam, and Gregory Soyez. The anti- k_r jet clustering algorithm. *JHEP*, 04:063, 2008.
- [9] Kihyuk Sohn, Honglak Lee, and Xinchen Yan. Learning structured output representation using deep conditional generative models. In C. Cortes, N. Lawrence, D. Lee, M. Sugiyama, and R. Garnett, editors, *Advances in Neural Information Processing Systems*, volume 28. Curran Associates, Inc., 2015.
- [10] Diederik P. Kingma and Max Welling. Auto-encoding variational bayes. *CoRR*, abs/1312.6114, 2014.
- [11] Manzil Zaheer, Satwik Kottur, Siamak Ravanbakhsh, Barnabás Póczos, Ruslan Salakhutdinov, and Alexander J. Smola. Deep sets. *CoRR*, abs/1703.06114, 2017.
- [12] Francesco Locatello, Dirk Weissenborn, Thomas Unterthiner, Aravindh Mahendran, Georg Heigold, Jakob Uszkoreit, Alexey Dosovitskiy, and Thomas Kipf. Object-centric learning with slot attention. *CoRR*, abs/2006.15055, 2020.
- [13] Harold. W. Kuhn. The Hungarian method for the assignment problem. *Naval research logistics quarterly*, 2:83–97, 1955.
- [14] Arthur Gretton, Karsten M. Borgwardt, Malte J. Rasch, Bernhard Schölkopf, and Alexander Smola. A kernel two-sample test. *J. Mach. Learn. Res.*, 13(null):723–773, mar 2012.
- [15] Diederik P Kingma and Jimmy Ba. Adam: A method for stochastic optimization. *arXiv preprint arXiv:1412.6980*, 2014.